Computers in Biology and Medicine 109 (2019) 263–271

Contents lists available at ScienceDirect

Computers in Biology and Medicine

journal homepage: www.elsevier.com/locate/compbiomed

Corneal deformation amplitude analysis for keratoconus detection through compensation for intraocular pressure and integration with horizontal thickness profile

Edileuza Leão[a,b,e,*], Tsang Ing Ren[a,e], João M. Lyra[b,e], Aydano Machado[c,e], Robert Koprowski[f], Bernado Lopes[j,k], Riccardo Vinciguerra[g], Paolo Vinciguerra[h], Cynthia J. Roberts[i], Ahmed Elsheikh[k,l,m], Katarzyna Krysik[n], Renato Ambrósio Jr.[d,j,e]

[a] Centro de Informática (CIn) - Universidade Federal de Pernambuco (UFPE) - v. Jornalista Aníbal Fernandes, Cidade Universitária, 50740-560, Recife, PE, Brazil
[b] Universidade Estadual de Ciências da Saúde de Alagoas (UNCISAL), Brazil
[c] Instituto de Computação (IC) - Universidade Federal de Alagoas (UFAL), Brazil
[d] Federal University of the State of Rio de Janeiro, Brazil
[e] Brazilian Study Group of Artificial Intelligence and Corneal Analysis (BrAIn), Brazil
[f] Department of Biomedical Computer Systems, University of Silesia, Faculty of Computer Science and Materials Science, Institute of Computer Science, Brazil
[g] Royal Liverpool and Broadgreen University Hospitals NHS Trust, UK
[h] Istituto Clinico Humanitas IRCCS, Italy
[i] Department of Ophthalmology Visual Science and Department of Biomedical Engineering, The Ohio State University, Columbus, OH, USA
[j] Department of Ophthalmology of Federal University of São Paulo, São Paulo, Brazil
[k] School of Engineering, University of Liverpool, Liverpool, UK
[l] National Institute for Health Research (NIHR) Biomedical Research Centre for Ophthalmology, Moorfields Eye Hospital NHS Foundation Trust and UCL Institute of Ophthalmology, London, UK
[m] School of Biological Science and Biomedical Engineering, Beihang University, Beijing, China
[n] Department of Ophthalmology with Paediatric Unit, St. Barbara Hospital, Trauma Center, Sosnowiec, Poland

ARTICLE INFO

Keywords:
Keratoconus
Image processing
Biomechanics
Intraocular pressure

ABSTRACT

Background: The Corvis ST provides measurements of intraocular pressure (IOP) and a biomechanically-corrected IOP (bIOP). IOP influences corneal deflection amplitude (DA), which may affect the diagnosis of keratoconus. Compensating for IOP in DA values may improve the detection of keratoconus.
Methods: 195 healthy eyes and 136 eyes with keratoconus were included for developing different approaches to distinguish normal and keratoconic corneas using attribute selection and discriminant function. The IOP compensation is proposed by dividing the DA by the IOP values. The first approaches include DA compensated for either IOP or bIOP and other parameters from the deformation corneal response (DCR). Another approach integrated the horizontal corneal thickness profile (HCTP). The best classifiers developed were applied in a validation database of 156 healthy eyes and 87 eyes with keratoconus. Results were compared with the current Corvis Biomechanical Index (CBI).
Results: The best biomechanical approach used the DA values compensated by IOP (Approach 2) using a linear discriminant function and reached AUC 0.954, with a sensitivity of 88.2% and a specificity of 97.4%. When thickness horizontal profile data was integrated (Approach 4), the best function was the diagquadratic, resulting in an AUC of 0.960, with a sensitivity of 89.7% and a specificity of 96.4%. There was no significant difference in the results between approaches 2 and 4 with the CBI in the training and validation databases.
Conclusions: By compensating for the IOP, and with the horizontal thickness profile included or excluded, it was possible to generate a classifier based only on biomechanical information with a similar result to the CBI.

* Corresponding author. Centro de Informática (CIn) - Universidade Federal de Pernambuco (UFPE) - v. Jornalista Aníbal Fernandes, Cidade Universitária, 50740-560, Recife, PE, Brazil.
E-mail address: edileuza.leao@uncisal.edu.br (E. Leão).

https://doi.org/10.1016/j.compbiomed.2019.04.019
Received 5 December 2018; Received in revised form 25 January 2019; Accepted 20 April 2019

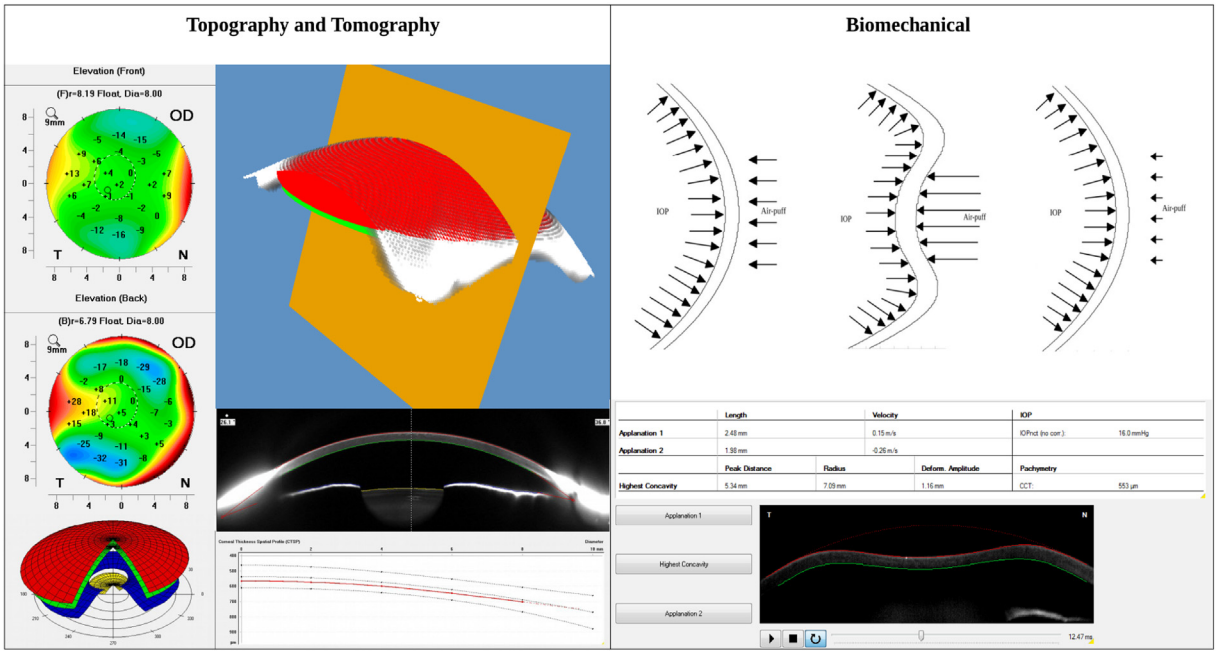

Fig. 1. Examples of different methods to evaluate the cornea using tomography, topography and biomechanical measurements.

1. Introduction

Keratoconus is a progressive, non-inflammatory, corneal disorder that is characterized by gradual loss and compression of collagen fibrils, developing a progressive thinning and a conical corneal protrusion [1]. In the early stages of the disease, contact lenses are commonly prescribed, however, with the progression of the disease surgical options may become necessary such as corneal transplantation [2]. There are several methods available to evaluate keratoconus including those based on measuring corneal topography [3,4], corneal tomography [5] and corneal biomechanics [6–12], Fig. 1.

Corneal topography [13] and tomography [14] measure corneal thickness and elevation. Today, it is believed that prior to corneal thinning and steepening, changes in biomechanical properties take place [15], therefore there is a need to develop biomechanical indices capable of detecting pre-clinical keratoconus prior to the development of changes in corneal shape characteristics and without the need for thickness information [16].

Corvis ST (Oculus Optikgerte GmbH, Wetzlar, Germany) is a device that evaluates corneal biomechanical response using a high-speed Scheimpflug camera [17] that takes 140 2D cross-sectional images of the cornea in 31 ms during deformation under an external air puff. The device records the images of corneal movement and estimates the intraocular pressure (IOP) from the first applanation data. Corvis ST also measures several biomechanical parameters related to the deformation corneal response (DCR) and horizontal corneal thickness profile (HCTP). This data is limited to the central horizontal cross-section of the cornea, which is different from the 3D tomography and topography measured by videokeratography devices. Earlier studies have evaluated corneal deformation recorded in Corvis ST images and separated the movement of the eye [18] from corneal response [19], here called the corneal deflection amplitude (DA).

In other earlier studies, corneal deformation led to estimation of a biomechanically-corrected IOP (bIOP) that was shown to be less affected by corneal biomechanical parameters than the Corvis ST reading [20,21]. The bIOP generation was based on finite element models that compensate for the effects of central corneal thickness (CCT) and corneal stiffness. While IOP is influenced by thickness [22,23], corneal deformation response is also influenced by IOP [24,25], and therefore it is important to investigate the impact of this influence on keratoconus detection. In doing so, it is proposed here to explore the effectiveness of deflection amplitude (DA), with or without compensation for IOP or bIOP, in keratoconus detection.

The present study aims to develop a classifier for the detection of keratoconus without reliance on thickness information using a method based on discriminant functions and attributes selection. After evaluating the best results, the thickness horizontal profile was considered to check if it can improve the accuracy of keratoconus detection.

2. Material

Corvis ST records a sequence of 140 cross-sectional images ($I = 140$) of the 8 mm central corneal zone during intraocular pressure measurement. Images have a resolution of $M \times N = 200 \times 576$ pixels. A training database was created for Corvis images obtained for 192 keratoconic eyes (26,880 images) and 263 healthy eyes (36,820 images), totaling 455 eyes ($E = 455$) of 451 patients. We also used a validation database for 119 keratoconic eyes and 206 healthy eyes, totaling 325 eyes ($E_v = 325$) of 324 patients.

Data was collected at the Instituto de Olhos Renato Ambrósio, Rio de Janeiro, Brazil and Vincieye Clinic in Milan, Italy. All patients underwent complete eye examination including ophthalmic health history and corrected visual acuity. Eyes with a history of ocular surgery or previous ocular illnesses were excluded from the study. The dataset was obtained following the Declaration of Helsinki.

3. Method

The method is divided into four phases where the images are processed, analyzed and a keratoconus detection classifier is developed:

1. Pre-processing
2. Determination of deflection amplitude intervals
3. Compensation of deflection amplitude for effects of IOP and bIOP
4. Development of classifiers

The block diagram on Fig. 2 shows the proposed method. Matlab was used for the entire development of the method and also MedCalc

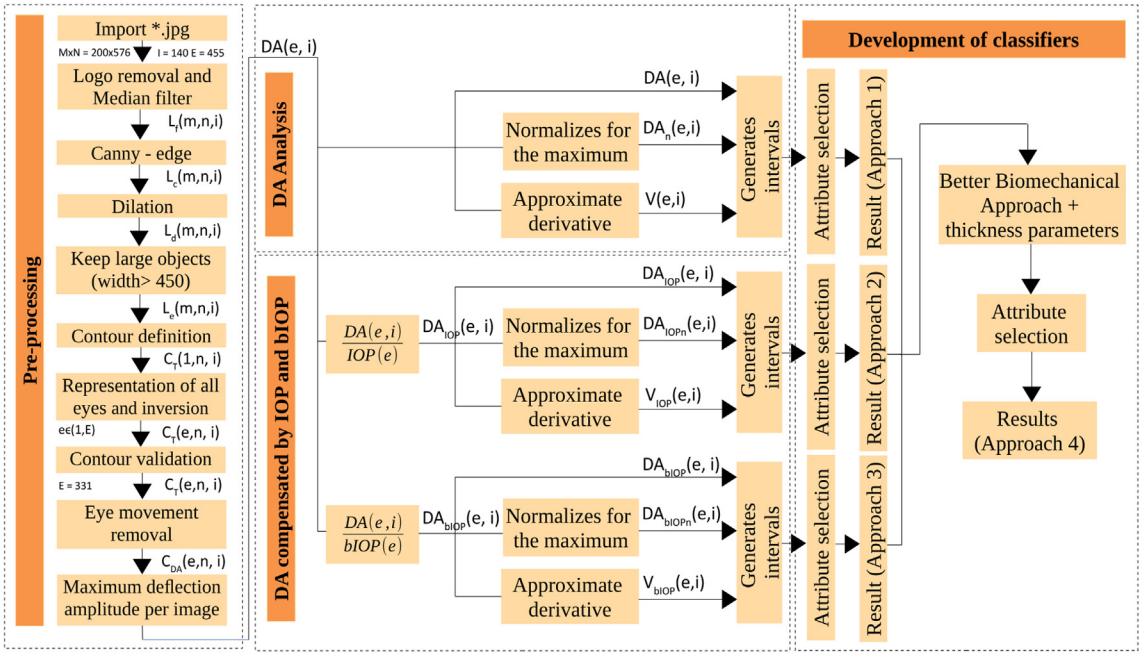

Fig. 2. Block diagram shows the proposed method.

for results performance.

3.1. Pre-processing

The intention of this phase is to pre-process the images to identify the corneal deflection amplitude (DA). This phase is based on and adapted from Refs. [19,26]. The input is a sequence of 140 images for each eye defined as cell array $L_{GRAY}\{e, i\}$ that each cell contains an image $[m, n]$, where e-rows to represent each eye $e\varepsilon(1, E)$, i-column defines the image sequence $i\varepsilon(1, I)$, and each cell contains a matrix where m-row $m\varepsilon(1, M)$ and n-column $n\varepsilon(1, N)$ of the image. Initially, a pre-processing step is applied to remove the logo from each image and a median filter with a mask hi of size 3 is applied $M_{hi} \times N_{hi} \times I_{hi} = 3 \times 3 \times 3$ which results in a sequence of images $L_f\{e, i\}$. Although [26] suggested a median filtering with a mask h sized $M_h \times N_h = 200 \times 576$ pixels, choosing a mask hi of size 3 proved to be a more suitable option, considering the size of the distortions and artifacts that frequently appear on the images.

The filtered images $L_f\{e, i\}$ are processed using the Canny [27] edge detection method, with an automatic threshold and a Gaussian filter with standard deviation of 2, resulting in $L_c\{e, i\}$. Several threshold values were tested. Using a high value the cornea was not entirely detected and using a small value brought excessive noise to the image. The ideal value is variable for each image. Several values for the standard deviations of the Gaussian filter were tested, values greater than 2 deforms the shape of the cornea. Empirically we obtained the value of two as an ideal value for visualizing the corneal format. The images undergoes an image morphological operation of dilation with a Structural Element (SE) $M_{SE} = 3 \times 3$ pixels, resulting in $L_d\{e, i\}$. Objects of width greater than 450 pixels were kept, that way the noises were eliminated resulting in $L_e\{e, i\}$.

The upper corneal curvature is identified in $L_e = \{e, i\}$ as the first blank point of each column in each image, which generates a matrix of the contours $C_T(e, n, i)$. The contour include the response of the eyeball $C_{EM}(e, n, i)$, the deflection amplitude of the cornea $C_{DA}(e, n, i)$ and the initial corneal contour $C_1(e, n, 1)$:

$$C_T(e, n, i) = C_{EM}(e, n, i) + C_{DA}(e, n, i) + C_1(e, n, 1) \quad (1)$$

The curvature of the left eyes was inverted to maintain the temporal nasal pattern. The contour $C_T(e, n, i)$ cannot present any discontinuity point and the maximum displacement of the contour line was 5 pixels within the same image and 15 pixels between following series images. This rule was used for contour validation, eliminating exams. After validation, the training database had 195 healthy eyes and 136 eyes with keratoconus, and E changes to $E = 331$. Validation database reduced to 243 eyes $E_v = 243$, 156 healthy eyes and 87 eyes with keratoconus. Only those exams that have passed the validation will be used for the development of the classifiers.

The eyeball movement $C_{EM}(e, n, i)$ was removed according to Refs. [19,26] using the average of 10 points from the extremities of the corneal curvature to linear interpolation. Such process involves determining the straight line passing through the points (n_l, f_l) and (n_r, f_r), where n_l and n_r are the extremities of the contour, f_l is 1 and f_r is N. Therefore the deflection amplitude was calculated as follows:

$$C_{DA}(e, n, i) = C_T(e, n, i) - C_{EM}(e, n, i) - C_1(e, n, 1) \quad (2)$$

Where:

$$C_{EM}(e, n, i) = f_l + (f_r - f_l).\frac{n - n_l(e, i)}{n_r(e, i) - n_l(e, i)} \quad (3)$$

$$f_l = 1\, f_r = N \quad (4)$$

and

$$n_l(e, i) = \frac{1}{10}\sum_{n=1}^{10} C_T(e, n, i) \quad (5)$$

$$n_r(e, i) = \frac{1}{10}\sum_{n=N-9}^{N} C_T(e, n, i) \quad (6)$$

The maximum $C_{DA}(e, n, i)$ value for each i was calculated, generating the signal of the deflection amplitude $DA(e, i)$ for each patient. Fig. 3 shows the deflection amplitude in the segmented image. Although the edge of the lower cornea curvature is detected by the proposed Canny method, this curvature is not used in the article.

$$DA(e, i) = max(C_{DA}(e, n, i)) \quad (7)$$

The $DA(e, i)$ is the sequence of maximum deflections at each image, arranged in a time series, named DA signal. Fig. 4 shows deflection amplitude signal for all exams. The next two phases of the method propose an analysis of the intervals of this signal and its variations.

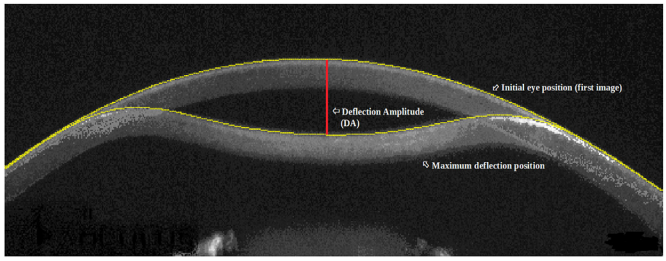

Fig. 3. Example of a cornea image showing the initial eye position, the maximum deflection position and the deflection amplitude (DA) represented by the line in red.

3.2. Determination of deflection amplitude intervals

The parameters obtained from Corvis related the amplitude of deflection are: the DA maximum and DA values at the applanation moments, however a more detailed analysis of the complete deflection amplitude signal is proposed here. The proposal is to observe deflection amplitude values at different moments of the exam, defining time intervals. In addition to the actual values of deflection amplitude $DA(e, i)$, the analysis of the intervals are also proposed for two variations of this signal: $DA_n(e, i)$ and $V(e, i)$.

The goal is to evaluate the deflection amplitude pattern with respect to time analyzing the deflection amplitude values intervals. Initially, all values are analyzed then the first half, the second half, the first third, and so forth. Such procedure divides the deflection amplitude signal up to 20 parts, defining a set of s-intervals, $s\varepsilon(1, S)$, where S is the sum of the arithmetic progression 1,2, …,19,20, then $S = 210$:

$$Intervals(1{:}\ S) = [(1{:}\ I);\ (1{:}\ round(I/2));\ (round(I/2) + 1{:}\ I);\ \ldots (18{*}round(I/20) + 1{:}\ 19{*}round(I/20));\ (19{*}round(I/20) + 1{:}\ I)] \quad (8)$$

An experimental analysis was performed to empirically define an ideal number of divisions and that number was 20, which is representative and not computationally expensive, higher values were tested, but presented computationally expensive. Each interval has its calculated median. The mean was also evaluated although the median presented better results. This procedure generates $R_{DA}(e, s)$, which consists of 210 median values based on intervals of the signal $DA(e, i)$.

$$R_{DA}(e, s) = median(DA(e, i)),\ \forall\ i\varepsilon Intervals(s) \quad (9)$$

It is also proposed to analyze the signal $DA_n(e, i)$, which is the normalization of the values of $DA(e, i)$ by the maximum value in each patient. Using the aforementioned method, $R_{DA_n}(e, s)$ was generated, consisting of 210 median values based on intervals of the signal $DA_n(e, i)$.

$$DA_n(e, i) = \frac{DA(e, i)}{max(DA(e))} \quad (10)$$

$$R_{DA_n}(e, s) = median(DA_n(e, i)),\ \forall\ i\varepsilon Intervals(s) \quad (11)$$

Deflection velocity is calculated through the approximation of the derivative of the DA signal. Corvis only analyzes the velocity values at the moments of applanation. The same interval analysis is once again proposed for the velocity signal $V(e, i)$ that generates $R_V(e, s)$:

$$V(e, i) = \begin{cases} DA(e, i+1) - DA(e, i) & if \quad i < I \\ 0 & other \end{cases} \quad (12)$$

$$R_V(e, s) = median(V(e, i)),\ \forall\ i\varepsilon Intervals(s) \quad (13)$$

This section generates the $R_{DA}(e, s)$, $R_{DA_n}(e, s)$, $R_V(e, s)$ median values that are used for the classifier development.

3.3. Compensation of deflection amplitude for effects of IOP and bIOP

This paper brings a compensation of the intraocular pressure (IOP) and the biomechanically-compensated IOP (bIOP) [20,21] upon the deflection amplitude values. Since IOP can influence deflection amplitude, the evaluations proposed here are intended to verify this possibility by analyzing keratoconus classification results. Intervals of deflection amplitude values compensated by IOP and bIOP, and the normalized signal and for the velocity were used, following the same methodology previously applied.

The intraocular pressure compensation is achieved by dividing the signal values of the deflection amplitude by the IOP value in each exam, generating the $DA_{IOP}(e, i)$:

$$DA_{IOP}(e, i) = \frac{DA(e, i)}{IOP(e)} \quad (14)$$

The deflection amplitude compensated by the corrected IOP (bIOP) is calculated in the same way, generating the signal $DA_{bIOP}(e, i)$:

$$DA_{bIOP}(e, i) = \frac{DA(e, i)}{bIOP(e)} \quad (15)$$

The proportion of the signal is analyzed normalizing the signal of each patient by its maximum value, generating the signals $DA_{IOPn}(e, i)$ and $DA_{bIOPn}(e, i)$:

$$DA_{IOPn}(e, i) = \frac{DA_{IOP}(e, i)}{max(DA_{IOP}(e))} \quad (16)$$

$$DA_{bIOPn}(e, i) = DA_{IOPn}(e, i) \quad (17)$$

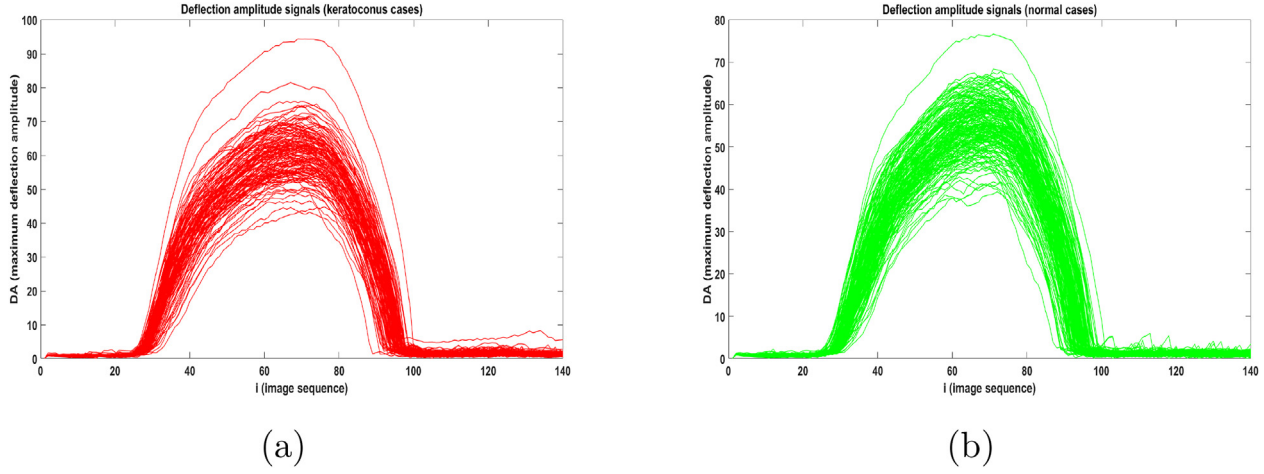

(a) (b)

Fig. 4. (a) Deflection amplitude signal for keratoconic eyes. (b) Deflection amplitude signal for healthy eyes.

Velocity calculation is also proposed for values compensated by IOP and bIOP, generating the signals: V_{IOP} and V_{bIOP}.

$$V_{IOP}(e, i) = \begin{cases} DA_{IOP}(e, i+1) - DA_{IOP}(e, i) & if \quad i < I \\ 0 & other \end{cases} \tag{18}$$

$$V_{bIOP}(e, i) = \begin{cases} DA_{bIOP}(e, i+1) - DA_{bIOP}(e, i) & if \quad i < I \\ 0 & other \end{cases} \tag{19}$$

The same method of interval analysis is applied to the signals of the deflection amplitude after compensation, generating: $R_{DA_{IOP}}(e, s)$, $R_{DA_{bIOP}}(e, s)$, $R_{DA_{IOPn}}(e, s)$, $R_{DA_{bIOPn}}(e, s)$, $R_{V_{IOP}}(e, s)$ and $R_{V_{bIOP}}(e, s)$.

$$R_{DA_{IOP}}(e, s) = median(DA_{IOP}(e, i)), \ \forall \ i \varepsilon Intervals(s) \tag{20}$$

$$R_{DA_{bIOP}}(e, s) = median(DA_{bIOP}(e, i)), \ \forall \ i \varepsilon Intervals(s) \tag{21}$$

$$R_{DA_{IOPn}}(e, s) = median(DA_{IOPn}(e, i)), \ \forall \ i \varepsilon Intervals(s) \tag{22}$$

$$R_{DA_{bIOPn}}(e, s) = median(DA_{bIOPn}(e, i)), \ \forall \ i \varepsilon Intervals(s) \tag{23}$$

$$R_{V_{IOP}}(e, s) = median(V_{IOP}(e, i)), \ \forall \ i \varepsilon Intervals(s) \tag{24}$$

$$R_{V_{bIOP}}(e, s) = median(V_{bIOP}(e, i)), \ \forall \ i \varepsilon Intervals(s) \tag{25}$$

These median values are used for the classifiers development, which is presented in the following section.

3.4. Development of classifiers

Four approaches to classifier development are proposed based on attribute selection using wrapper methods [28] and Fishers discriminant [29], Fig. 5. The intention is to evaluate the predictive power of the deflection values with or without IOP and bIOP compensation. Attribute selection was by forward selection with wrapper methods or Fishers discriminant with leave-one-out-cross-validation (LOOCV) evaluating linear end quadratic types. The criterion for feature selection is through maximization of AUC.

The selection method proposed is the forward selection since all the selection approaches have many similar attributes and it is our goal to identify the attributes that are really relevant for keratoconus classification. The six forms present in Matlab of the discriminant function were applied to classifiers development: linear, quadratic, diagquadratic, diaglinear, pseudolinear and pseudoquadratic, using LOOCV on the training database.

The first aim is to develop the best possible classifier based only on the biomechanics of the cornea, including 35 output parameters [17,20,30–32] already measured by the Corvis, but excluding the thickness parameters: IOP, bIOP, A1 Time, A1 Velocity, A1 Deflection Amp, A1 Deflection Length, A1 Deflection Area, A1 dArc Length, A1 Deformation Amp, A2 Time, A2 Velocity, A2 Deflection Amp, A2 Deflection Length, A2 Deflection Area, A2 dArc Length, A2 Deformation Amp, HC Time, HC Deflection Amp, HC Deflection Length, HC Deflection Area, HC dArc Length, HC Deformation Amp, Radius, Max Inverse Radius, Integrated Radius, Whole Eye Movement Max mm, Whole Eye Movement Max ms, Def Amp Max, DA Ratio Max 2 mm, DA Ratio Max 1 mm, Deflection Amp Max mm, Deflection Amp Max ms, dArcLengthMax, Peak Dist and SPA1, Table 1.

The first approach involves the median of the intervals of the deflection amplitude $R_{DA}(e, s)$ (210 attributes) and the signals derived from it: median of the normalized signal intervals $R_{DA_n}(e, s)$ (210 attributes) and median of the velocity signal intervals $R_V(e, s)$ (210 attributes) along with the aforementioned Corvis attributes including IOP (35 attributes), totaling 665 attributes for selection. The second approach is to analyze the intervals of the signals related to deflection compensated by IOP $R_{DA_{IOP}}(e, s)$, $R_{DA_{IOPn}}(e, s)$ and $R_{V_{IOP}}(e, s)$ (630 attributes) adding the Corvis ST output parameters but without including IOP and bIOP (33 attributes) and totaling 663 attributes. The third approach is similar to the second except for consideration of bIOP instead of IOP, also totaling 663 attributes.

Finally, in Approach 4, the thickness horizontal profile was then considered through inclusion of three parameters obtained by the Corvis related to the thickness: Pachy(m), PachySlope(m) and Arth. A new classifier based on the same attribute selection method was developed combining these thickness parameters with the result of the best biomechanical approach. The definition of the best biomechanical classifier was based on the AUC resulting from the cross-validation in the training database. The best biomechanical approach and Approach 4 are applied to the validation database for assessment of keratoconus detection accuracy. Fig. 5 demonstrates the four classifier development approaches. In order to evaluate the results of the classifiers, a cutoff

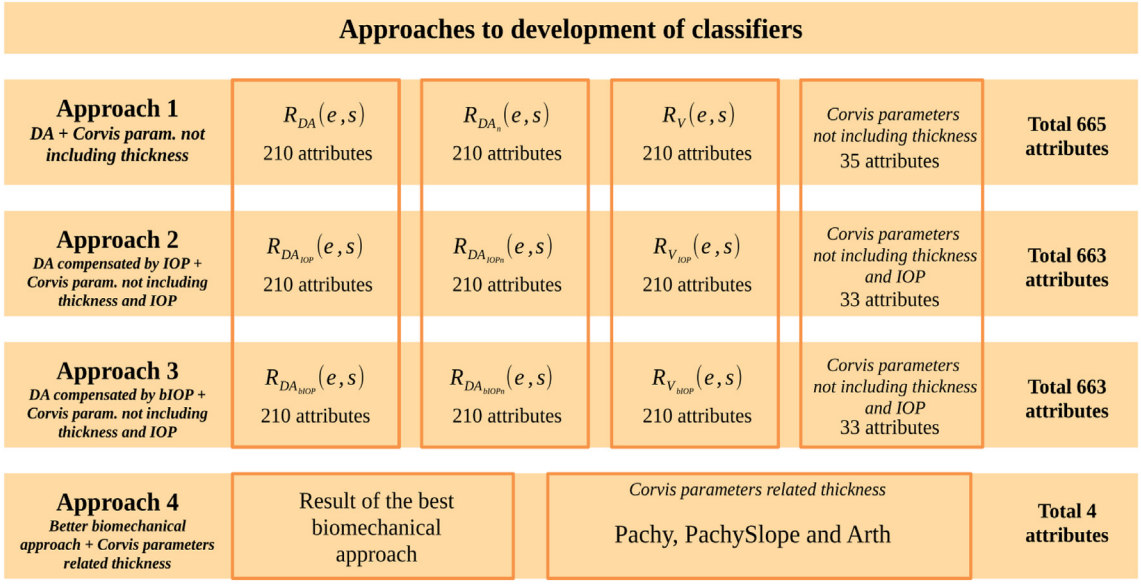

Fig. 5. The four approaches to classifiers development based on attribute selection. Approach 1 gathering intervals regarding deflection amplitude signal and Corvis ST output parameters, not including thickness information. Approach 2 gathering intervals regarding deflection amplitude signal compensated by IOP and Corvis ST output parameters, not including thickness and IOP information. Approach 3 gathering intervals regarding deflection amplitude signal compensated by bIOP and Corvis ST output parameters, not including thickness and IOP information. Approach 4 gathering the best previous approach with thickness horizontal profile.

Table 1
Description of Corvis output parameters.

Parameters short name	Description
IOP	Intraocular pressure [mmHg]
bIOP	Biomechanically-corrected Intraocular pressure
A1 Time	First applanation time [ms]
A1 Velocity	Velocity at first applanation [m/s]
A1 Deflection Amp	Deflection amplitude at first applanation [mm]
A1 Deflection Length	Deflection length at first applanation [mm]
A1 Deflection Area	Deflection area at first applanation [mm^2]
A1 dArc Length	Change in arc length (length along the curved line) at first applanation [mm]
A1 Deformation Amp	Deformation amplitude at first applanation [mm]
A2 Time	Second applanation time [ms]
A2 Velocity	Velocity at second applanation [m/s]
A2 Deflection Amp	Deflection amplitude at second applanation [mm]
A2 Deflection Length	Deflection length at second applanation [mm]
A2 Deflection Area	Deflection area at second applanation [mm^2]
A2 dArc Length	Change in arc length (length along the curved line) at second applanation [mm]
A2 Deformation Amp	Deformation amplitude at second applanation [mm]
HC Time	Highest concavity time [ms]
HC Deflection Amp	Deflection amplitude at highest concavity [mm]
HC Deflection Length	Deflection length at highest concavity [mm]
HC Deflection Area	Deflection area at highest concavity [mm^2]
HC dArc Length	Change in arc length (length along the curved line) at highest concavity [mm]
HC Deformation Amp	Deformation amplitude at highest concavity [mm]
Radius	Corneal radius at time of highest concavity [mm]
Max Inverse Radius	The maximum inverse corneal radius [mmˆ-1]
Integrated Radius	Integrated radius (area under the inverse Radius curve vs. Time) [mmˆ-1]
Whole Eye Movement Max mm	The maximum whole eye movement [mm]
Whole Eye Movement Max ms	Time of the maximum whole eye movement [ms]
Def Amp Max	The maximum deformation amplitude [mm]
DA Ratio Max 2 mm	Ratio between deformation amplitude at apex and at 2 mm nasal and temporal
DA Ratio Max 1 mm	Ratio between deformation amplitude at apex and at 1 mm nasal and temporal
Deflection Amp Max mm	The maximum deflection amplitude [mm]
Deflection Amp Max ms	The maximum deflection amplitude time [ms]
dArcLengthMax	The maximum distance along the curved line [mm]
Peak Dist	Peak distance [mm]
SPA1	Adjusted pressure at (A1 - bIOP)/A1 deflection amplitude
Pachy	Pachymetry [μm]
PachySlope	Slope of the pachymetry [μm]
ARTh	Ambrsio relational thickness to the horizontal profile

point of 0.5 was standardized.

4. Results

For Approach 1, which involves intervals related to the deflection amplitude together with the Corvis ST output parameters, but not including the thickness, the selected attributes were:

- SPA1 [32].
- Interval 3/13 *DA*
- Interval 1/16 *DA*
- Interval 10/12 *V*
- Interval 12/12 *V*
- Interval 12/13 *V*

For Approach 2, which evaluates the deflection amplitude compensated by IOP together with the Corvis ST output parameters, but again excluding the thickness, the selected attributes were:

- A1 Deformation Amp(mm)
- A2 Deflection Length
- A2 Deflection Amp(mm)
- DA Ratio Max 2 mm
- SPA1
- Interval 3/4 DA_{IOP}
- Interval 6/6 V_{IOP}
- Interval 2/8 V_{IOP}
- Interval 5/10 V_{IOP}
- Interval 9/12 V_{IOP}

For Approach 3, which seeks to eliminate the influence of bIOP, the selected attributes were:

- SPA1
- Interval 1/9 DA_{bIOP}
- Interval 12/16 DA_{bIOP}
- Interval 5/5 V_{bIOP}
- Interval 5/10 V_{bIOP}
- Interval 3/16 V_{bIOP}

The results of the classifier developed in the training database in each approach with the best discriminant function and for each biomechanical approach are shown in Table 2. The table also shows results obtained with the Corvis Biomechanical Index (CBI) [31].

Table 2
Results of CBI parameter in training database and results of discriminant functions for each biomechanical approach.

Approaches	TP	FP	FN	TN	SEN	SPC	ACC	AUC
CBI								
CBI	185	10	16	120	0.882	0.949	0.921	0.950
Approach 1								
Linear	186	9	25	111	0.816	0.954	0.897	0.914
Approach 2								
Linear	190	5	16	120	0.882	0.974	0.937	0.954
Approach 3								
Linear	182	13	17	119	0.875	0.933	0.909	0.938

SPC-specificity, SEN-sensitivity, ACC-accuracy, AUC-area under curve.
TP-true positive, TN-true negative, FP-false positive and FN-false negative.

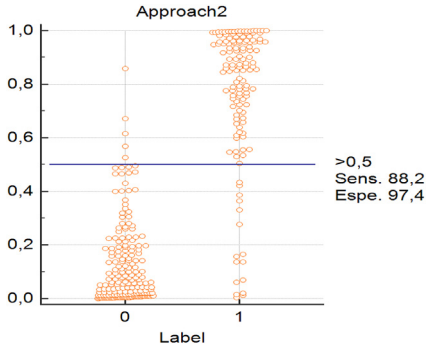

Fig. 6. DotPlot Approach 2 - DA compensated by the IOP with Corvis ST output parameters, not including thickness.

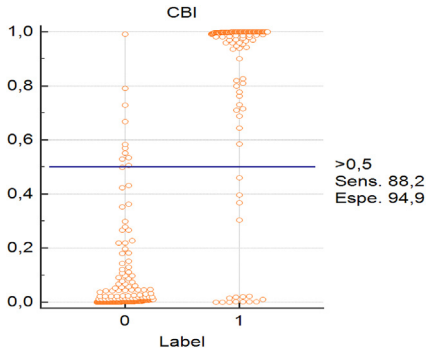

Fig. 7. DotPlot CBI.

The AUC of the linear functions adopted in Approaches 1, 2 and 3 were 0.914, 0.954 and 0.938, respectively. The linear classifier of Approach 2 presented the best AUC and was therefore considered the best biomechanical approach. Fig. 6 shows a dot plot for Approach 2, along with a comparison with the CBI performance, Fig. 7.

In Approach 4, thickness parameters; Pachy, PachySlope and Arth, were added to those considered in Approach 2, leading to the following list of selected attributes:

- PachySlope
- The results of Approach 2

The classifier generated with the DiagQuadratic function in Approach 4 reached an AUC of 0.960, a specificity of 0.964, a sensitivity of 0.897 and accuracy of 0.937, as presented in Table 3. Fig. 8 shows the dot plot for this approach. The integration of the horizontal thickness profile was also tested in the other approaches, but did not produce better results. Fig. 9 shows comparisons of the Receiver Operating Characteristic (ROC) [33] curves for the four approaches and the CBI.

The best biomechanical approach (Approach 2) and Approach 4, which integrates the horizontal thickness profile were applied to the validation database. Both Approaches 2 and 4 result in AUC 0.868, but

Table 3
Results of Approach 4 that gathers the best biomechanical approach result and thickness horizontal profile in training database.

Functions	TP	FP	FN	TN	SEN	SPC	ACC	AUC
Linear/PseudoLinear	190	5	16	120	0,882	0,974	0,937	0,951
Quadratic/PseudoQuad.	184	11	14	122	0,897	0,944	0,924	0,957
DiagLinear	190	5	17	119	0,875	0,974	0,934	0,957
DiagQuadratic	188	7	14	122	0,897	0,964	0,937	0,960

SPC-specificity, SEN-sensitivity, ACC-accuracy, AUC-area under curve.
TP-true positive, TN-true negative, FP-false positive and FN-false negative.

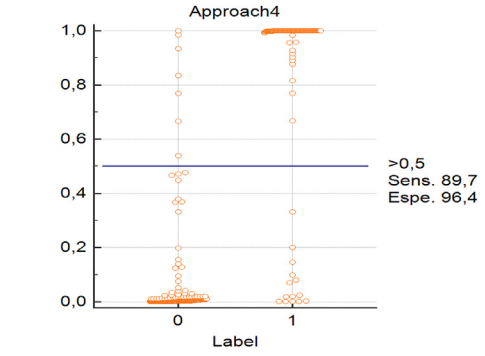

Fig. 8. DotPlot Approach 4 - DA compensated by the IOP with Corvis ST output parameters including thickness horizontal profile.

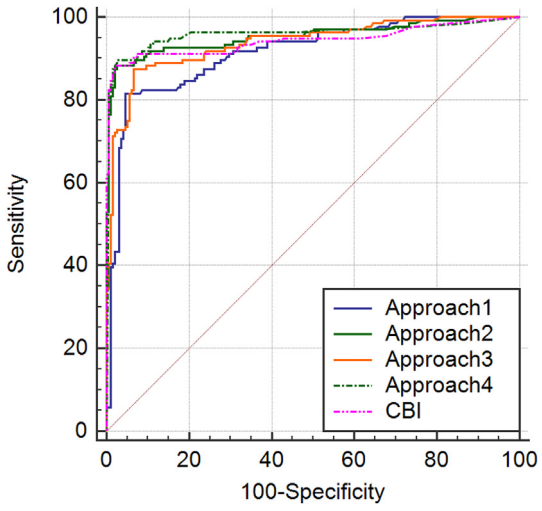

Fig. 9. ROC curves comparison of the four approaches for classifier development along with the CBI index in the training database.

Table 4
Results of CBI, Approach 2 and Approach 4 in the validation database.

Functions	TP	FP	FN	TN	SEN	SPC	ACC	AUC
CBI								
CBI	150	6	24	63	0,724	0,962	0,877	0,874
Approach 2								
Linear	150	6	39	48	0,552	0,962	0,815	0,868
Approach 4								
DiagQuadratic	151	5	39	48	0,552	0,968	0,819	0,868

SPC-specificity, SEN-sensitivity, ACC-accuracy, AUC-area under curve.
TP-true positive, TN-true negative, FP-false positive and FN-false negative.

there was a difference in accuracy with 0.815 for Approach 2, 0.819 for Approach 4 and 0.874 for the CBI, as presented in Table 4. In order to verify the difference between the CBI and Approaches 2 and 4, the significance level was calculated. As shown in Table 5, there was no significant difference in any of the analyzed pairs, considering a significance level of 0.05.

5. Discussions and conclusions

The study of corneal biomechanics is clinically relevant in screening for mild keratoconus and form fruste keratoconus. The present work created classifiers for detection of keratoconus based on deflection amplitude values (DA) with and without compensation for effect of IOP and bIOP. The aim of this study was to develop a classifier with only biomechanical information of the cornea. One of the approaches tested

Table 5
Comparison of the significance level between CBI and each approach.

Comparison pairs	Significance level
Training database	
CBI ~Approach 1	P = 0,0655
CBI ~Approach 2	P = 0,5035
CBI ~Approach 3	P = 0,7092
CBI ~Approach 4	P = 0,3224
Approach 1 ~Approach 2	P = 0,0007
Approach 1 ~Approach 3	P = 0,0302
Approach 1 ~Approach 4	P = 0,0004
Approach 2 ~Approach 3	P = 0,0466
Approach 2 ~Approach 4	P = 0,4392
Approach 3 ~Approach 4	P = 0,0377
Validation database	
CBI ~Approach 2	P = 0,7828
CBI ~Approach 4	P = 0,8016
Approach 2 ~Approach 4	P = 0,9093

in the study (Approach 2) was considered the best possible biomechanical approach, which provided results that showed no significant differences from those of the Corvis Biomechanical Index (CBI) [31]. That is despite the fact that the CBI included information on the horizontal thickness profile. However, when the HCTP information was included in Approach 4, a significance level higher than 0.05 was maintained but with only a small improvement in accuracy, confirming the importance of using thickness as proposed in Ref. [16]. As the results without IOP compensation (Approach 1) are significantly lower than the results of the compensated values (Approaches 2 and 3) we can confirm that the compensation proposal made through the division, which considers the individual pressure variation, has brought considerable improvement to detection of keratoconus.

An important observation is the difference in results with compensation of the deflection amplitude (DA) for the effects of IOP and bIOP. Approach 1 – which involves DA signal intervals together with the Corvis ST output parameters; presented a significant difference in accuracy against all other approaches, confirming the improvement caused by compensation for IOP or bIOP. Comparing Approach 2 – DA signal intervals compensated by IOP and Corvis ST output parameters; to Approach 3 – DA signal intervals compensated by bIOP and Corvis ST output parameters, it is noticed that there was no significant difference between the values computed with compensation for IOP and bIOP.

The work [26] evaluates corneal vibration values for keratoconus classification with 92% accuracy, confirming that it is useful to evaluate corneal vibration. Since Approach 4 presented accuracy greater than 93% in training database, it would be interesting to investigate if the result of the corneal vibration values evaluation after IOP treatment would increase accuracy in Ref. [26]. As to the BAD [34] and TBI [35] indexes, it is a temptation to join output parameters from various devices to achieve better prediction rates. BAD – index that links topography and tomography; and the TBI – index that links tomography and biomechanics; are the indices that achieve better rates for detection of keratoconus presenting AUC of 1.00 and AUC of 0.996, respectively, for the reported cases. As a suggestion for future works, we propose to join the new biomechanical information generated in this study with information from other classical methods of corneal analysis for tomography, which include more detailed thickness information, and topography as well as adding clinical data to future analysis.

Acknowledgment

Aydano Machado acknowledge financial support from National Council for Scientific and Technological Development (CNPq) - Grant# 310601/2016-9.

References

[1] Y. Rabinowitz, Keratoconus, Surv. Ophthalmol. 42 (4) (1998) 297–319, https://doi.org/10.1016/S0039-6257(97)00119-7.
[2] V. Jhanji, N. Sharma, R.B. Vajpayee, Management of keratoconus: current scenario, Br. J. Ophthalmol. 95 (8) (2011) 1044–1050, https://doi.org/10.1136/bjo.2010.185868.
[3] J. Bühren, Corneal topography and keratoconus diagnostics with Scheimpflug photography, Ophthalmologe 111 (10) (2014) 920–926, https://doi.org/10.1007/s00347-013-2962-3.
[4] B.T. Lopes, I. De Carvalho Ramos, M.Q. Salomão, A. Laura, C. Canedo, R. Ambrósio, Perfil paquimétrico horizontal para a detecção do ceratocone Horizontal pachymetric profile for the detection of keratoconus, Rev. Bras. Oftalmol. 74 (6) (2015) 382–385, https://doi.org/10.5935/0034-7280.20150080.
[5] B.T. Lopes, I.C. Ramos, M.Q. Salomão, F.P. Guerra, S.C. Schallhorn, J.M. Schallhorn, R. Vinciguerra, P. Vinciguerra, F.W. Price, M.O. Price, D.Z. Reinstein, T.J. Archer, M.W. Bellin, A.P. Machado, R. Ambrósio, Enhanced tomographic assessment to detect corneal ectasia based on artificial intelligence, Am. J. Ophthalmol. (2018), https://doi.org/10.1016/j.ajo.2018.08.005.
[6] R. Shetty, R.M.M.A. Nuijts, P. Srivatsa, C. Jayadev, N. Pahuja, M.C. Akkali, A. Sinha Roy, Understanding the correlation between tomographic and biomechanical severity of keratoconic corneas, BioMed Res. Int. 2015 (2015) 294197, , https://doi.org/10.1155/2015/294197.
[7] C. Ye, M. Yu, G. Lai, V. Jhanji, Variability of corneal deformation response in normal and keratoconic eyes, Optom. Vis. Sci. 92 (7) (2015), https://doi.org/10.1097/OPX.0000000000000628 e149–e153.
[8] M. Francis, N. Pahuja, R. Shroff, R. Gowda, H. Matalia, R. Shetty, E.J.R. Nelson, A.S. Roy, Waveform analysis of deformation amplitude and deflection amplitude in normal, suspect, and keratoconic eyes, J. Cartaract Refract. Surg. 43 (10) (2017) 1271–1280, https://doi.org/10.1016/j.jcrs.2017.10.012.
[9] R. Ambrósio Jr., F.F. Correia, B. Lopes, M.Q. Salomão, A. Luz, D.G. Dawson, A. Elsheikh, R. Vinciguerra, P. Vinciguerra, C.J. Roberts, Corneal biomechanics in ectatic diseases: refractive surgery implications, Open Ophthalmol. J. 11 (Suppl-1) (2017) 176–193, https://doi.org/10.2174/1874364101711010176 M2).
[10] B.T. Lopes, C.J. Roberts, A. Elsheikh, R. Vinciguerra, P. Vinciguerra, S. Reisdorf, S. Berger, R. Koprowski, R. Ambrósio, Repeatability and reproducibility of intraocular pressure and dynamic corneal response parameters assessed by the Corvis ST, J. Ophthalmol. 2017 (2017) 4–8, https://doi.org/10.1155/2017/8515742.
[11] G. Scarcelli, S. Besner, R. Pineda, S.H. Yun, Biomechanical characterization of keratoconus corneas ex vivo with brillouin microscopy, Investig. Ophthalmol. Vis. Sci. 55 (7) (2014) 4490–4495, https://doi.org/10.1167/iovs.14-14450.
[12] R. Mercatelli, F. Ratto, F. Rossi, F. Tatini, L. Menabuoni, A. Malandrini, R. Nicoletti, R. Pini, F.S. Pavone, R. Cicchi, Three-dimensional mapping of the orientation of collagen corneal lamellae in healthy and keratoconic human corneas using SHG microscopy, J. Biophot. 10 (1) (2017) 75–83, https://doi.org/10.1002/jbio.201600122.
[13] Y.S. Rabinowitz, P.J. McDonnell, Computer-assisted corneal topography in keratoconus, J. Refract. Surg. 5 (6) (1989) 400–408, https://doi.org/10.3928/1081-597X-19891101-10.
[14] R. Ambrósio, A.L.C. Caiado, F.P. Guerra, R. Louzada, A.S. Roy, A. Luz, W.J. Dupps, M.W. Belin, Novel pachymetric parameters based on corneal tomography for diagnosing keratoconus, J. Refract. Surg. 27 (10) (2011) 753–758, https://doi.org/10.3928/1081597X-20110721-01.
[15] C.J. Roberts, W.J. Dupps, Biomechanics of corneal ectasia and biomechanical treatments, J. Cataract Refract. Surg. 40 (6) (2014) 991–998, https://doi.org/10.1016/j.jcrs.2014.04.013 arXiv:15334406.
[16] R. Vinciguerra, R. Ambrósio, C.J. Roberts, A. Elsheikh, B. Lopes, P. Vinciguerra, J. Steinberg, S.J. Linke, Should the Corvis biomechanical index (CBI) include corneal thickness parameters? J. Refract. Surg. 34 (3) (2018) 213–216, https://doi.org/10.3928/1081597X-20180103-01.
[17] R. Ambrósio, I. Ramos, A. Luz, F.C. Faria, A. Steinmueller, M. Krug, M.W. Belin, C.J. Roberts, Dynamic ultra high speed Scheimpflug imaging for, Assess. Corneal Biomech. Prop. 72 (2) (2013) 99–102, https://doi.org/10.1590/S0034-72802013000200005.
[18] R. Koprowski, S. Wilczyński, A. Nowinska, A. Lyssek-Boron, S. Teper, E. Wylegala, Z. Wróbel, Quantitative assessment of responses of the eyeball based on data from the Corvis tonometer, Comput. Biol. Med. 58 (2015) 91–100, https://doi.org/10.1016/j.compbiomed.2015.01.006.
[19] R. Koprowski, A. Lyssek-Boron, A. Nowinska, E. Wylegala, H. Kasprzak, Z. Wróbel, Selected parameters of the corneal deformation in the Corvis tonometer, Biomed. Eng. Online 13 (1) (2014) 55, https://doi.org/10.1186/1475-925X-13-55.
[20] A.A. Joda, M.M.S. Shervin, D. Kook, A. Elsheikh, Development and validation of a correction equation for Corvis tonometry, Comput. Methods Biomech. Biomed. Eng. 19 (9) (2015) 943–953, https://doi.org/10.1080/10255842.2015.1077515.
[21] A. Eliasy, K.-J. Chen, R. Vinciguerra, O. Maklad, P. Vinciguerra, R. Ambrósio, C.J. Roberts, A. Elsheikh, Ex-vivo experimental validation of biomechanically-corrected intraocular pressure measurements on human eyes using the CorVis ST, Exp. Eye Res. 175 (2018) 98–102, https://doi.org/10.1016/J.EXER.2018.06.013.
[22] A. Kotecha, E.T. White, J.M. Shewry, D.F. Garway-Heath, The relative effects of corneal thickness and age on Goldmann applanation tonometry and dynamic contour tonometry, Br. J. Ophthalmol. 89 (12) (2005) 1572–1575, https://doi.org/10.1136/bjo.2005.075580.
[23] J. Liu, C.J. Roberts, Influence of corneal biomechanical properties on intraocular pressure measurement: quantitative analysis, J. Cataract Refract. Surg. 31 (1) (2005) 146–155, https://doi.org/10.1016/j.jcrs.2004.09.031.

[24] T. Huseynova, G.O. Waring IV, C. Roberts, R.R. Krueger, M. Tomita, Corneal biomechanics as a function of intraocular pressure and pachymetry by dynamic infrared signal and scheimpflug imaging analysis in normal eyes, Am. J. Ophthalmol. 157 (4) (2014) 885–893, https://doi.org/10.1016/j.ajo.2013.12.024.

[25] F.J. Bao, M.L. Deng, Q.M. Wang, J.H. Huang, J. Yang, C. Whitford, B. Geraghty, A. Yu, A. Elsheikh, Evaluation of the relationship of corneal biomechanical metrics with physical intraocular pressure and central corneal thickness in exvivo rabbit eye globes, Exp. Eye Res. 137 (May) (2015) 11–17, https://doi.org/10.1016/j.exer.2015.05.018.

[26] R. Koprowski, R. Ambrósio, Quantitative assessment of corneal vibrations during intraocular pressure measurement with the air-puff method in patients with keratoconus, Comput. Biol. Med. 66 (2015) 170–178, https://doi.org/10.1016/j.compbiomed.2015.09.007.

[27] J. Canny, A computational approach to edge detection, IEEE Transactions on Pattern Analysis and Machine Intelligence PAMI-8, 1986, pp. 679–698, , https://doi.org/10.1109/TPAMI.1986.4767851 (6).

[28] R. Kohavi, G.H. John, Wrappers for feature subset selection, Artif. Intell. 97 (1–2) (1997) 272–324, https://doi.org/10.1016/S0375-9474(97)00711-2.

[29] R.A. Fishert, The use of multiple measurements in taxonomic problems, Annals of Eugenics, vol. 7, 1936, pp. 179–188.

[30] H.R. Vellara, D.V. Patel, Biomechanical properties of the keratoconic cornea: a review, Clin. Exp. Optom. 98 (1) (2015) 31–38, https://doi.org/10.1111/cxo.12211.

[31] R. Vinciguerra, R. Ambrósio, A. Elsheikh, C.J. Roberts, B.T. Lopes, E. Morenghi, C. Azzolini, P. Vinciguerra, Detection of keratoconus with a new biomechanical index, J. Refract. Surg. 32 (12) (2016) 803–810, https://doi.org/10.3928/1081597X-20160629-01.

[32] C.J. Roberts, A.M. Mahmoud, J.P. Bons, A. Hossain, A. Elsheikh, R. Vinciguerra, P. Vinciguerra, R. Ambrósio, Introduction of two novel stiffness parameters and interpretation of air PuffInduced biomechanical deformation parameters with a dynamic scheimpflug analyzer, J. Refract. Surg. 33 (4) (2017) 266–273, https://doi.org/10.3928/1081597X-20161221-03.

[33] E.R. DeLong, D.M. DeLong, D.L. Clarke-Pearson, Comparing the areas under two or more correlated receiver operating characteristic curves: a nonparametric approach, Biometrics 44 (3) (1988) 837, https://doi.org/10.2307/2531595 arXiv:1608.07910.

[34] F.F. Correia, I. Ramos, B. Lopes, M.Q. Salomão, A. Luz, R.O. Correa, M.W. Belin, R. Ambrósio, C. Ff, I. Ramos, B. Lopes, Topometric and tomographic indices for the diagnosis of keratoconus, Int. J. Keratoconus Ectatic Corneal Dis. 1 (2) (2012) 92–99, https://doi.org/10.5005/jp-journals-10025-1018.

[35] R. Ambrósio, B.T. Lopes, F. Faria-Correia, M.Q. Salomão, J. Bühren, C.J. Roberts, A. Elsheikh, R. Vinciguerra, P. Vinciguerra, Integration of scheimpflug-based corneal tomography and biomechanical assessments for enhancing ectasia detection, J. Refract. Surg. 33 (7) (2017) 434–443, https://doi.org/10.3928/1081597X-20170426-02.